https://doi.org/10.5194/essd-2025-195
Preprint. Discussion started: 12 June 2025
© Author(s) 2025. CC BY 4.0 License.

Open Access Earth System Science Data Discussions

Quantifying the spatial-temporal patterns of land-atmosphere water, heat and CO_2 flux exchange over the Tibetan Plateau from an observational perspective

Binbin Wang[1,2,5,6,7], Yaoming Ma[1,2,3,4,5,6,7*], Zeyong Hu[8], Weiqiang Ma[1,2, 4,5,6,7], Xuelong Chen[1,2,5,6,7], Cunbo Han[1,2,5,6,7], Zhipeng Xie[1,2,5,6,7], Yuyang Wang[9], Maoshan Li[10], Bin Ma[1,5,6,7], Xingdong Shi[1,4,7], Weimo Li[1,4], Zhengling Cai[1,4]

[1]State Key Laboratory of Tibetan Plateau Earth System, Resources and Environment (TPESRE), Institute of Tibetan Plateau Research, Chinese Academy of Sciences, Beijing 100101, China;

[2]College of Earth and Planetary Sciences, University of Chinese Academy of Sciences, Beijing 100049, China;

[3]College of Hydraulic & Environmental Engineering, China Three Gorges University, Yichang 443002, China;

[4]College of Atmospheric Science, Lanzhou University, Lanzhou 730000, China;

[5]National Observation and Research Station for Qomolongma Special Atmospheric Processes and Environmental Changes, Dingri 858200, China;

[6]Kathmandu Center of Research and Education, Chinese Academy of Sciences, Beijing 100101, China;

[7]China-Pakistan Joint Research Center on Earth Sciences, Chinese Academy of Sciences, Islamabad 45320, Pakistan;

[8]Key Laboratory of Land Surface Process and Climate Change in Cold and Arid Regions, Northwest Institute of Eco-Environment and Resources, Chinese Academy of Sciences, Lanzhou, 730000, China;

[9]College of Grassland Science and Technology, China Agricultural University, Beijing, 100193,China;

[10]School of Atmospheric Sciences, Chengdu University of Information Technology, Chengdu 610225, China

Corresponding authors: Binbin Wang (wangbinbin@@itpcas.ac.cn); Yaoming Ma (ymma@itpcas.ac.cn); Address: Building 3, Courtyard 16, Liucui Road, Chaoyang District, Beijing City, China. Zip code: 100101.

https://doi.org/10.5194/essd-2025-195
Preprint. Discussion started: 12 June 2025
© Author(s) 2025. CC BY 4.0 License.

Open Access Earth System Science Data Discussions

Abstract

Land-atmosphere (LA) interaction process, through the turbulent exchange of water, heat and CO_2 flux, significantly influences regional micro-climates, local water cycles, energy budgets, and ecosystem dynamics. The Tibetan Plateau (TP), characterized by vast extent, high elevation, strong solar radiation and convection, as well as extreme weather fluctuations, has been under-explored due to the scarcity of LA interaction stations, particularly in the western and northern regions. To address this gap, this study introduces a newly constructed research and observation platform, which consists of 16 planetary boundary layer towers, spans diverse landscapes and covers dynamic meteorological conditions, with average annual air temperature, wind speed and liquid precipitation ranging from -3.5 to 18.5 °C, 0.6 to 5.6 m s^{-1}, and 43 mm to 2164 mm. Elevation correlates significantly with all meteorological variables, highlighting a strong spatial heterogeneity distribution patterns of LA coupling. The turbulent flux of water and heat show clear seasonal variations, with highest sensible heat flux (*SH*) in April-May and largest latent heat flux (*LE*) in July-August. Further, most stations report negative net ecosystem exchange (*NEE*) values, ranging from -3.2 g C m^{-2} a^{-1} to -174.3 g C m^{-2} a^{-1}, and function as carbon sinks. However, Medog station, locating in the densely forested Yarlung Zangbo valley, functions as a carbon source which is most probably related to the vegetation destruction and human activities. *LE* is significantly and closely correlated with *SH*, *NEE* and ecosystem respiration, indicating strong coupling between water, heat and carbon fluxes. Precipitation as well as soil water content provide favorable moisture sources and show significance in the water-carbon coupling process. The observation and research platform and the quality-controlled high-temporal resolution data provide valuable in situ measurements for studying water-heat-carbon interactions, validating numerical models and satellite algorithms, and offering ground truth for research on hydrological, meteorological, and ecological responses to global climate change.

Key worlds: Land-atmosphere turbulent flux, spatial-temporal variations, comprehensive observation and research platform, Tibetan Plateau

https://doi.org/10.5194/essd-2025-195
Preprint. Discussion started: 12 June 2025
© Author(s) 2025. CC BY 4.0 License.

1 Introduction

Land-atmosphere (LA) interaction, which governs the flux exchanges of energy, water, and CO_2 between the Earth's surface and the atmosphere, are pivotal in shaping regional water cycles, climate dynamics, and ecosystem changes [*Gentine et al., 2019; Y Ma et al., 2023; Santanello et al., 2018; Seo and Ha, 2022; Y Zhang et al., 2024*]. The thermal contrasts between distinct landscapes—such as land vs. water, mountain vs. valley, and ocean vs. land—drive both regional circulations, like lake-land and mountain-valley breezes, and large-scale atmospheric motions, including monsoons [*Gerken et al., 2014; Wu and Zhang, 1998; Wu et al., 2023*]. These interactions are forced by distinct LA interaction processes, which can further influence air pollution dispersion, atmospheric moisture transport, regional convergence/divergence, redistribution of clouds and precipitation as well as ecosystem evolution and carbon budget [*Bei et al., 2018; Friedlingstein et al., 2022; Suni et al., 2015; Zhu et al., 2017*]. For example, the intensified coupling of soil moisture and land surface temperature can exacerbate droughts and heatwaves in northern East Asia (1980-2019) [*Seo and Ha, 2022*], where soil moisture deficits reduce evapotranspiration (*ET*), amplifying heatwave conditions, particularly in areas with sparse vegetation. Further, the LA water and heat coupling can even impact the intricate non-linear feedback between *ET* and cloud water content, especially in transitional zones where uncertainties remain under energy-limited and water-limited *ET* regimes [*Y Zhang et al. [2024*]. Under global climate warming, the carbon absorption/release capacity through LA interactions by abrupt permafrost thaw, plant uptake and ecosystem respiration have also been debated globally, especially over the data scarce regions [*Turetsky et al., 2020; Y Wang et al., 2023b; Wei et al., 2021*]. Therefore, understanding and quantifying the full spectrum of LA coupling through the in situ measurements of energy, water, and CO_2 flux is essential for comprehending the Earth system's response to climate change.

Understanding LA interactions through coordinated, multidisciplinary, and multi-scale observations is crucial for addressing global challenges such as water resource management, land-use planning, climate change, and ecosystem preservation. In this context, key global initiatives—such as the First International Satellite Land Surface Climatology Project Field Experiment (United States) [*P J Sellers et al., 1992*], the Hydrologic Atmospheric Pilot Experiment (France, Niger) [*André et al., 1986; Goutorbe et al., 1997*], the Northern Hemisphere Climate Processes Land Surface Experiment (Sweden) [*Halldin et al., 1999*], the Boreal Ecosystem–Atmosphere Study (Canada) *[P Sellers et al., 1995]*, the Inner Mongolia Semiarid Grassland Soil–Vegetation–Atmosphere Interaction and the Heihe River Basin Field Experiment (China) [*Liu et al., 2018; Lü et al., 1997*]—have provided foundational insights into LA interactions and have advanced parameterizations for climate models. Tibetan Plateau (TP), the world's largest and highest plateau, plays a particularly critical role in the climate and ecology dynamics. TP exerts significant influence on atmospheric processes, generating thermal disturbances that affect circulation patterns, weather, and climate not only in China and East Asia but also globally[*Wu and Zhang, 1998; Ye and Wu, 1998*]. For example, mesoscale system vortices and shear lines created in the TP's atmospheric boundary layer can lead to extreme weather events, such as heavy rain and storms, impacting both the plateau and surrounding regions [*L Li et al., 2020; Xu and Chen, 2006*]. Thus, LA coupling and dynamics are important for the formation and development of weather systems. Over the past few decades, large-scale field activities and long-term observational experiments—such as QXPMEX, TIPEX-I, TIPEX-II, TIPEX-III, JICA, GAME/Tibet, and CAMP/Tibet—have greatly enhanced our understanding of land surface processes in the TP *[Huang et* al., 2023; Y Ma et al., 2023], and these efforts have also helped refine climate model parameterization, improving our ability to predict TP's climatic effects. However, the stations for measuring heat, water and CO_2 exchange are concentrated mostly in the east and still rarely distributed over the vast northern and western regions, hindering our understanding on its spatial distribution and total amounts of heat, water and CO_2 flux. Given the growing challenges posed by global climate change, accurately measuring and modeling LA interaction processes is more critical than ever, and such efforts are essential for predicting climate extremes, managing water resources, and supporting sustainable ecology [Suni et al., 2015].

LA interaction station has decades of experiences in analyzing the dynamic LA interaction parameters, the seasonal variations of turbulent flux and the driving forces behind them [Y Ma et al., 2005; Y Ma et al., 2018; Y Ma et al., 2023; Wang et al., 2011; Yang et al., 2008]. Meanwhile, comprehensive LA interaction stations have been widely used to assess and to evaluate water and heat turbulent fluxes derived from satellite algorithms and numerical simulations. The water-carbon coupled biophysical model (PML-V2) has been used to generate a data set for *ET* and its components over the period 1982–2016. Validation using eddy covariance (EC) measurements confirmed the reliability of the results, yielding an average *ET* value of 353 ± 24 mm yr^{-1}. Simultaneously, based on EC measurements, soil moisture, and soil texture data, [Ling Yuan et al., 2021] developed an improved *ET* model and created a monthly *ET* data set covering the period from 1982 to 2018 [L. Yuan et al., 2024]. Validation at nine EC stations demonstrated that the model outperforms previous studies, with an average annual ET value of approximately 346.5 ± 13.2 mm yr^{-1}, which is highly consistent with the results of [N Ma and Zhang, 2022]. However, factors influencing the inter-annual variations in *ET* exhibit significant biases and uncertainties, especially for data-scarce western and northern regions. As for carbon function, TP contains extensive permafrost and a variety of landscapes, including alpine meadows, alpine steppes, alpine shrubs, alpine wetlands, forests, and alpine deserts, which have a significant impact on the carbon sink/source function of the region, and shows important ecological and environmental consequences. Recent studies indicate that most alpine meadows on the TP function as carbon sinks, with values ranging from -430 to -12.5 g C m^{-2} a^{-1}, and some alpine steppe areas act as weak carbon sources [Y Wang et al., 2023a; Wei et al., 2021]. Specifically, alpine grasslands exhibit a weaker carbon sink function, with values ranging from -206.9 to -17.1 g C m^{-2} a^{-1} whilst shrub lands show even lower carbon sink values, ranging from -89.5 to -40.7 g C m^{-2} a^{-1}. Marshes display considerable variability in carbon fluxes, with values ranging from -187 ± 29 g C m^{-2} a^{-1} in Shenzha to -478 g C m^{-2} a^{-1} in Haibei [Qi et al., 2021; Zhao et al., 2005]. Therefore, by synthesizing EC and climate data from multiple sites across the TP, we can understand clearly the spatial patterns of water, heat, CO_2 flux and identify the mechanisms that control them.

This study introduces a comprehensive observation and research platform for LA water, heat, and CO_2 flux exchange over the TP (Figure S1 and Table S1) and provides a preliminary analysis of data collected from 15 stations spanning more than 2 years recently, especially over the data-limited regions of western and northern TP. The objectives are to address the following scientific questions: (1) What are the characteristics of land-atmosphere water, heat, and CO_2 flux exchange across different landscapes of the TP? (2) What are the spatial and temporal distributions of water, heat, and CO_2 flux, and what factors influence these variations? Specifically, the development of the observation platform, instrument configuration, and standardized data processing methods introduced in the "Methods". The

https://doi.org/10.5194/essd-2025-195
Preprint. Discussion started: 12 June 2025
© Author(s) 2025. CC BY 4.0 License.

preliminary results and discussions on the spatial-temporal variations of meteorological variables, energy budget components, and CO_2 flux exchange are illustrated in the "Results and Discussion".

2 The observation platform and methods

2.1 Introduction of observation platform and instruments configuration

The LA interaction process is essential in driving regional air motion and water cycles and influencing weather and climate change. The EC system is widely used as a direct measure—or ground truth—for estimating energy and material flux at the LA interface. Over time, long-term and quasi-continuous EC networks have been established across various ecosystems and land covers globally, including networks in North and South America (AmeriFlux and Fluxnet-Canada), Europe (EuroFlux and CarboEurope), Asia (ChinaFlux and AsiaFlux), and Australia (OzFlux) [*Baldocchi, 2014; Yu et al., 2024*]. The TP has an area of 2.6 million km^2 and presents extreme environmental conditions, such as high solar radiation, low temperatures, large diurnal temperature variations, limited precipitation, nutrient-poor soils, shallow soil profiles, and short growing seasons. These factors contribute to strong convection and intense weather variations. However, TP is also characterized as a region lacking EC stations, particularly in the arid and semi-arid northern and western parts. To address this gap, the Institute of Tibetan Plateau Research, Chinese Academy of Sciences (ITPCAS), established six comprehensive and long-term LA interaction stations in remote and data-scarce regions of TP gradually since 2004 [*Y M Ma et al., 2008*], including QOMOS (the Qomolangma Atmospheric and Environmental Observation and Research Station, CAS), NAMORS (the Nam Co Monitoring and Research Station for Multisphere Interactions, CAS), SETORS (the Southeast Tibet Observation and Research Station for the Alpine Environment, CAS), NADORS (the Ngari Desert Observation and Research Station, CAS), MAWORS (the Muztagh Ata Westerly Observation and Research Station, CAS), and Shuanghu. Since 2019, the 6 stations were upgraded with new sonic anemometer and gas analyzer sensors gradually (CSAT3 and LI7500DS, details in Table S1), enhancing the measurement capabilities. The instrumentation and long-term data at 5 stations covering 2006–2021 can be found in [*Y Ma et al., 2020*] and [*Y Ma et al., 2024*].

Furthermore, the Second Tibetan Plateau Expedition and Research Program (STEP) in 2019 has expanded the network, adding 10 additional LA interaction stations, including Medog, Qamdo, Mangkam, Mangai, Baingoin, Nyima, Jyirong, Burang, Coqen, Lhasa, especially in the remote western and northern regions. The integrated eddy turbulence devices (IRGASON, Campbell; CSAT3 & LI7500RS in Lhasa), capable of measuring high-frequency (10 Hz) quantities of sonic temperature, water, CO_2, and three-dimensional winds, have been used. This expansion resulted in the creation of the Third Pole Environment Integrated Three-dimensional Observation and Research Platrom (TPEITORP, observation platform for short hereafter) for measuring water, heat, and CO_2 flux over the TP [*Y Ma et al., 2023*]. All the stations have a 20 m planetary boundary layer (PBL) tower measurements (in Lhasa the configuration height is 40 m), including traditional variables such as air pressure, liquid precipitation, infrared land surface temperature, four-component radiation, soil temperature and moisture at multi-layers, air temperature, air humidity and wind at 5 layers, as well as turbulent flux of water, heat and CO_2. The details of the instrument configuration, station locations, and photographs are provided in Table 1 and Figure 1, respectively. In-situ measurements from these stations, with updated systems, were utilized to analyze the seasonal and diurnal variations of water, heat, and CO_2 exchange, as well as the energy budget and carbon source/sink dynamics across

https://doi.org/10.5194/essd-2025-195
Preprint. Discussion started: 12 June 2025
© Author(s) 2025. CC BY 4.0 License.

contrasting ecosystems and climates. A detailed illustration of the observational environments at 16 stations are as follows.

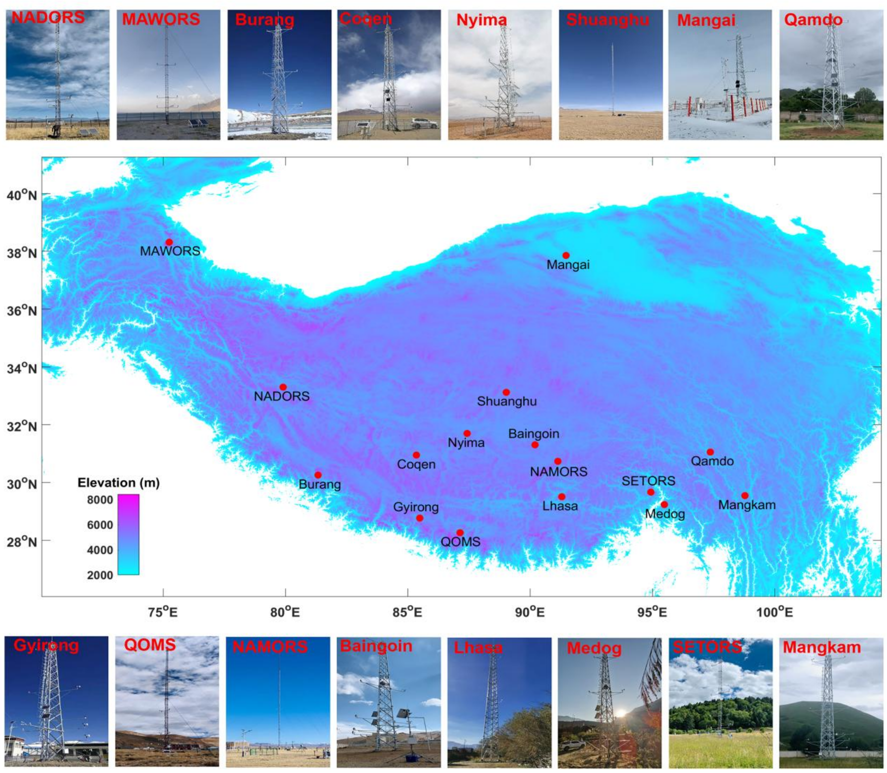

Figure 1. The locations and photos of 16 LA interaction stations composing the comprehensive observation and research platform over the TP. (All the photos have been taken by the authors)

QOMOS station is located in Rongbuk Valley, north of Mt. Everest, with a flat observation field dominated by barren land and sparse vegetation. NAMORS station, on the southeast bank of the third largest lake (Nam Co) in TP, is covered by alpine meadow. Both QOMOS and NAMORS have in situ EC and PBL tower systems that have been in operation since 2005, with sensors upgraded in 2019. SETORS station, located in a mountain valley in the southeast TP, is covered with dense vegetation (50–60 cm high). The EC and PBL systems were first installed in 2007 and fully upgraded in 2020. NADORS station, in grassland near Ritu County and Bangong Co, has had an EC system and an automatic weather station (AWS) since 2008, with a new 20 m PBL tower and an EC system installed in 2020. MAWORS station, located near Mustag Mountain and Karakori Lake in Xinjiang, is influenced by westerly winds. The station has been equipped with an EC system since 2010, and both EC and PBL systems were updated in October 2020. Shuanghu station, located 3 km north of Shuanghu County, has been operational since 2012, with a typical alpine grassland surface. The original EC system is still in use, with new EC and PBL systems added in 2021.

https://doi.org/10.5194/essd-2025-195
Preprint. Discussion started: 12 June 2025
© Author(s) 2025. CC BY 4.0 License.

Table 1. Overview of instruments configuration and settings at 16 stations, including observation variables, instrument sensors, observational heights, latitude (lat), longitude (lon), altitude (alt) and landscape at each station.

<table>
<tr><th>Variables</th><th>Sensors (Manufacturers)</th><th>Heights</th><th>Stations (lat, lon, alt, landscape)</th></tr>
<tr><td>Air temperature and humidity</td><td>HMP155A-L (Vaisala)</td><td>1.5, 2, 4, 10, and 20 m</td><td rowspan="8">1. QOMOS (28.36°N, 86.95°E, 4276 m, Alpine desert);
2. NAMORS (30.77°N, 90.98°E, 4730 m, Alpine steppe);
3. SETORS (29.77°N, 94.73°E, 3327 m, Alpine meadow);
4. NADORS (33.39°N, 79.7°E, 4270 m, Alpine desert);
5. MAWORS (38.41°N, 75.05°E, 3668 m, Alpine desert);
6. Shuanghu (33.22°N, 88.83°E, 4947 m, Alpine steppe);
7. Lhasa (40.01 °N, 116.38 °E, 3650 m, City)</td></tr>
<tr><td>Wind speed and direction</td><td>05103-L (R.M.Young)</td><td>1.5, 2, 4, 10, and 20 m</td></tr>
<tr><td>Air pressure</td><td>CS106 (Vaisala)</td><td>-</td></tr>
<tr><td>Radiations</td><td>CNR4 (Kipp & Zonen)</td><td>1.5 m</td></tr>
<tr><td>Precipitation</td><td>RG3 (Onset)</td><td>-</td></tr>
<tr><td>Soil temperature and moisture</td><td>CS655 (Campbell)</td><td>0.1, 0.2, 0.4, 0.8 and 1.6 m</td></tr>
<tr><td>Soil heat flux</td><td>HFP01 (Hukseflux)</td><td>0.1 and 0.2 m</td></tr>
<tr><td>Turbulent flux</td><td>CSAT3B (Campbell)；LI-7500DS (Li-COR)</td><td>Site specific</td></tr>
<tr><td>Air temperature and humidity</td><td>HMP155A (Vaisala)</td><td>1, 2, 4, 10 and 20 m</td><td rowspan="8">8. Medog (29.32°N, 95.29°E, 820 m, Forest);
9. Qamdo (31.15°N, 97.17°E, 3307 m, Alpine steppe);
10. Mangkam (29.64°N, 98.59°E, 3840 m, Alpine meadow);
11. Mangai (37.95°N, 91.7°E, 3073 m, Bare ground);
12. Baingoin (31.4°N, 90.01°E, 4709 m, Bare ground);
13. Nyima (31.79°N, 87.23 °E, 4573 m, Alpine steppe);
14. Jyirong (28.86 °N, 85.29 °E, 4140 m, Bare ground);
15. Burang (30.35 °N, 81.14 °E, 4113 m, Bare ground);
16. Coqen (31.04 °N, 85.16 °E, 4683 m, Alpine steppe);</td></tr>
<tr><td>Wind speed and direction</td><td>05103 (R.M.Young)</td><td>1, 2, 4, 10 and 20 m</td></tr>
<tr><td>Air pressure</td><td>PTB110 (Vaisala)</td><td>-</td></tr>
<tr><td>Radiations</td><td>CNR4 (Kipp & Zonen)</td><td>1.5 m</td></tr>
<tr><td>Precipitation</td><td>RG3 (Onset)</td><td>-</td></tr>
<tr><td>Soil temperature and moisture</td><td>CS655 (Campbell)</td><td>0.1, 0.2, 0.4, 0.8, 1.6 m</td></tr>
<tr><td>Soil heat flux</td><td>HFP01 (Hukseflux)</td><td>0.1 and 0.4 m</td></tr>
<tr><td>Turbulent flux</td><td>IRGASON (Campbell)</td><td>Site specific</td></tr>
<tr><td colspan="4">Notes: the heights of turbulent flux measurements from station number 1 to number 16 are 3.0 m, 3.77 m, 3.13 m, 3.7 m, 3 m, 3.2 m, 5 m, 5.5 m, 5.5 m, 3.5 m, 3.5 m, 5.5 m, 3.8 m, 3.5 m, 3.5 m and 40 m respectively. In Lhasa station, the heights of atmosphere variables at 5 layers are 2 m, 4 m, 8 m, 16 m, 32 m.</td></tr>
</table>

The stations of Medog, Qamdo, Mangkam, Mangai, Baingoin, Nyima, Jyirong, Burang, Coqen and Lhasa were gradually established till 2021 with support from STEP program. Medog, Qamdo, and Mangkam stations are located in the southeastern TP. Medog is located at the southern foot of the eastern Himalayas, near the Yarlung Zangbo River, with a steep terrain surrounded by tropical plants and crops. Qamdo is situated in the Changdu Meteorological Bureau's observation field, covered by grass at the top of hilly Changdu City. Mangkam is located at the Mangkang County Meteorological

https://doi.org/10.5194/essd-2025-195
Preprint. Discussion started: 12 June 2025
© Author(s) 2025. CC BY 4.0 License.

Bureau's external observation field, with a surface covered by 10 cm grass. Mangai station is in the northern part of the TP, with a Gobi desert landscape. The PBL tower and EC system were mounted on the Mangai Meteorological Bureau's external observation field. Baingoin, Nyima, and Coqen stations are located in the west-central TP, each with PBL and EC systems installed at their respective County Meteorological Bureau's observation fields. The land surfaces are bare ground, alpine meadow and alpine meadow, respectively. Jyirong and Burang, located north of the Himalayas, are covered by sparse vegetation and bare land, respectively. Lhasa station, constructed in 2020 and having a 40 m PBL tower, is located in field observation base of ITPCAS, with roads and low-level buildings surrounded.

These stations are distributed across various climatic and environmental regions, covering landscapes such as alpine desert, alpine steppe, alpine meadow, bare ground and city. Some stations, including Mangkam, Baingoin, Qamdo and Lhasa are situated in or adjacent to cities, thus they can be influenced by nearby human activities to some extent. The land surface properties (e.g., land cover, terrain, soil texture) and local climate vary significantly across stations, providing valuable data for generalizing LA interaction schemes across diverse environments and climates over the TP. These differences highlight the complexity of coupled LA interactions, the challenges in obtaining necessary data for model development, and the need for a comprehensive understanding of how land surface processes affect atmospheric conditions and climate predictability. After the construction of the observation platform in 2021, the instruments calibration and maintenance have been carried out twice a year, with field work distance of more than 5000 km and duration of more than 1 month each time. Our effort to maintain the observation platform aims to address the observational gaps in these data-scarce regions and to support studies on land surface processes, water cycles, and the environmental effects over the TP.

2.2 Methods for data processing and analyze

To study the spatial-temporal variations of meteorological variables and turbulent fluxes of water, heat and CO_2 at these stations and to analyzing the influencing factors over the different climatic and environmental conditions, 15 stations have been chosen in this study with an exception of Lhasa, which only captured the measurements during the daytime because of the power malfunction at night. We selected field measurements of more than 2 years, mostly covering the period of May 2021 to July 2023. The proportions of data coverage for meteorological variables and turbulent flux are close to 94% and 77%, respectively, with the least data integrity percentage of approximately 50% in Mangai station. Details of data coverage at each station can be found in Table S1 in supplementary material. By further considering the data loss resulting from instruments failure, human incorrect operation and others, precipitation measurements covering a complete year of June 2021 to July 2022 are used in this study, with precipitation data loss only in three stations: 20% in QOMS (Feb 1 – Feb 14, May 14 – Jun 1, 2022), 22% in NAMORS (Jan 1 – Mar 21, 2022), and 6% in SETORS (Feb 8 – Feb 12, Mar 27 – Apr 12, 2022). As rain gauge (RG3, Onset) only records liquid rain in warm seasons and does not capture solid precipitation in cold seasons, the missing data, mostly during winter months and before monsoon, does not affect the conclusions on variations in liquid precipitation in this study.

Currently, the meteorological variables are processed following several standardized procedures, and the abnormal values in the long term data series have been corrected or removed. For examples, the

https://doi.org/10.5194/essd-2025-195
Preprint. Discussion started: 12 June 2025
© Author(s) 2025. CC BY 4.0 License.

downward short wave radiation, that are higher than solar constant or lower than 0, and the meteorological variables, those does not show correct diurnal or seasonal variations due to power malfunctions or other interfering issues, have been carefully checked and removed. For turbulent heat flux, two types of open-path EC systems were used across the stations: CSAT3B and LI-7500DS (stations 1–7) and IRGASON (stations 8–16). Theses high frequency data were processed using standard EddyPro software, which includes standard procedures of spike removal, buoyancy flux conversion to sensible heat, double rotation, as well as ultrasonic virtual temperature correction and density (WPL) correction [*Massman and Lee, 2002; Mauder and Foken, 2006; Twine et al., 2000*]. Quality flags are applied to the flux estimates, considering steady state test and integral turbulence characteristics test [*Mauder et al., 2013*]. Net ecosystem change (*NEE*) is calculated as the difference between ecosystem respiration (*Re*) and gross primary productivity (*GPP*), where *Re* and *GPP* are the primary components of the carbon cycle. Flux partitioning estimates *GPP* and *Re* using the standard procedure of REddyProc package [*Wutzler et al., 2018*], where a temperature response function for *NEE* fluxes is used to represent *Re*, with *GPP* derived as the difference between *Re* and *NEE*. Nighttime *NEE* data with low friction velocity were filtered to avoid biases, and gaps were filled using the available meteorological data.

To understand the climatology and environmental conditions, the diurnal and seasonal variations of meteorological variables and turbulent flux have been estimated with low quality and obvious spikes removed. Monthly-averaged diurnal variations of meteorological variables and turbulent flux were used to mitigate the influence of missing data and to examine the spatial-temporal patterns across stations. The total annual values for *ET*, *NEE*, *GPP* and *Re* were obtained by summing the monthly values. Due to the instrument malfunction, carbon flux in Baingoin, NAMORS and QOMOS are ignored in this study. The energy budget ratio (*EBR*) and Bowen ratio (*Bo*) at each station were estimated to evaluate energy conditions and energy consumption. *EBR* ($EBR = \frac{\sum LE+SH}{\sum R_n - G}$) compares the cumulative sum of available energy inputs to the cumulative sum of turbulent energy outputs over an entire year. Available energy inputs include net radiation (R_n, W m^{-2}) and ground heat flux (G, W m^{-2}) while turbulent energy outputs include latent heat flux (*LE,* W m^{-2}) and sensible heat flux (*SH,* W m^{-2}). Net radiation can be measured by four components radiation sensors and is expressed as the difference between downward and upward shortwave ($R_{s\downarrow}$ and $R_{s\uparrow}$, W m^{-2}) and longwave radiation ($R_{l\downarrow}$ and $R_{l\uparrow}$), specifically: $R_n = R_{s\downarrow} + R_{l\downarrow} - R_{s\uparrow} - R_{l\uparrow}$. Bowen ratio ($Bo = \frac{SH}{LE}$) indicates the relative proportions of energy consumption between *SH* and *LE*. Typically, *Bo* is high under dry conditions and low under wet conditions.

3 Results and Discussions

3.1 The spatial-temporal variations of meteorological conditions

https://doi.org/10.5194/essd-2025-195
Preprint. Discussion started: 12 June 2025
© Author(s) 2025. CC BY 4.0 License.

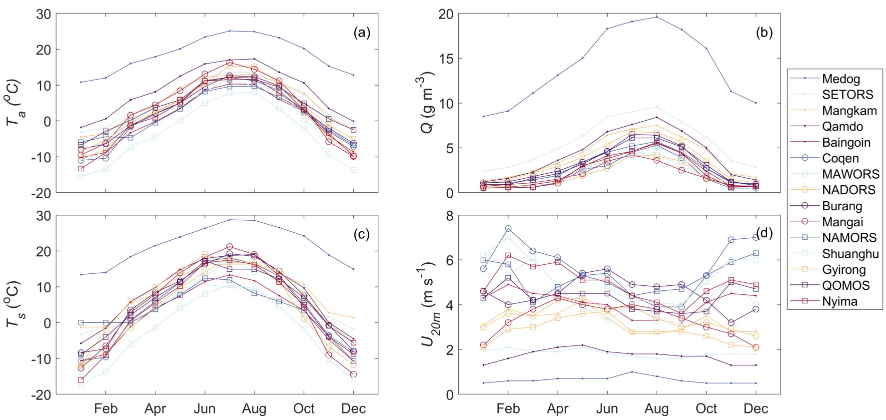

Figure 2. The seasonal variations of meteorological variables, including (a) air temperature (T_a), (b) air humidity (Q); (c) land surface temperature (T_s); (d) wind speed at 20 m height (U20m).

The 15 stations are distributed across diverse environments and climates, resulting in significant variations in the seasonal patterns of air temperature (T_a), air humidity (Q), wind speed (U_{20m}) and land surface temperature (T_s) (Figure 2 and Table 2). The details of seasonal variations of the monthly average and annual mean of air temperature, wind speed and absolute humidity at the 15 stations can be found in Table S2-S4. The annual average T_a, T_s, Q and U_{20m} span at ranges of -3.5~18.5 °C, -3.5~21.6 °C, 1.88~14.1 $g\,m^{-3}$ and 0.6~5.6 m s^{-1}, respectively. The annual average T_a shows strong positive correlations (r) with annual average T_s (r = 0.99) and downward long-wave radiation ($R_{l\downarrow}$, r = 0.84), and a notable negative correlation with downward short-wave radiation ($R_{s\downarrow}$, r = -0.72) (Figure S1). The high correlation with T_s indicates that strong LA coupling governs the spatial distribution of T_a, while the negative correlation with $R_{s\downarrow}$ reflects the impact of cloud cover, which reduces $R_{s\downarrow}$ but increases T_a. Additionally, the annual average T_a exhibits a significant negative correlation with elevation (r = -0.92). The highest annual average T_a (18.5°C) occurs at Medog station (820 m a.s.l.), while the lowest (−3.5°C) is observed at Shuanghu station (4947 m a.s.l.). Stations such as Qamdo (3307 m a.s.l.), SETORS (3327 m a.s.l.), Mangkam (3840 m a.s.l.), and Mangai (3073 m a.s.l.) have annual average values ranging from 5.2°C to 8.6°C, whereas stations above 4000 m have annual averages from −3.5°C to 3.9°C. Seasonal variations in T_a can also be influenced by climatic and environmental conditions. For example, despite similar elevations (around 3300 m a.s.l.) and low wind speeds (approximately 1.8 m s^{-1}), Qamdo shows larger annual value and amplitude in T_a than that in SETORS, and it may be attributed to the former's lower moisture condition as well as the strong "urban heat island" effect. Qamdo, having lower annual precipitation value, is located at a mountaintop grass land observation field in the city center, thus, relatively weak evaporated cooling and intense human activities and infrastructure may contribute to Qamdo's elevated T_a. Similarly, in Baingoin and NAMORS, despite their proximity and similar elevations, NAMORS experiences higher T_a from October to February and lower temperatures from March to August. Such variations are likely influenced by the large lake (Nam Co), which has a cooling effect in summer and a warming effect in winter.

Table 2. The annual average meteorological variables, soil water contents (*SM10* and *SM160* indicate soil moisture at 10 cm and 160 cm, respectively), *NEE*, *GPP*, *Re*, *ET*, *EBC* and *Bo* at 15 stations.

https://doi.org/10.5194/essd-2025-195
Preprint. Discussion started: 12 June 2025
© Author(s) 2025. CC BY 4.0 License.

Sites	T_a (℃)	Q (g m^{-3})	U_{20m} (m s^{-1})	T_s (℃)	*Prec* (mm)	SM 10 (%)	*SM* 160 (%)	*NEE* (g C $m^{-2}a^{-1}$)	*GPP* (g C $m^{-2}a^{-1}$)	*Re* (g C $m^{-2}a^{-1}$)	*ET* (mm)	*EBC* (-)	*Bo* (-)
Medog	18.5	14.1	0.6	21.6	2164	9 - 25	18 - 43	365	885	1193	571	1.04	0.46
SETORS	5.7	5.64	1.8	6.1	1053	32 - 42	20 - 50	-153	754	633	381	0.634	0.84
Mangkam	5.2	4.07	3.3	6.2	596	4 - 16	20 - 41	-121	454	192	345	0.683	1.09
Qamdo	8.6	4.3	1.7	9.0	456	4 - 14	8 - 19	-133	486	443	354	0.650	0.73
Baingoin	0.5	2.38	4.1	1.2	392	3 - 22	1 - 12	Nan	Nan	Nan	208	0.680	1.52
NAMORS	1.3	2.80	5.2	2.6	304	1 - 9	3 - 6	Nan	Nan	Nan	348	0.828	1.64
Shuanghu	-3.5	2.10	5.3	-3.5	246	1 - 10	9 - 38	-86	165	75	174	0.836	1.88
Gyirong	2.9	3.53	2.8	4.3	237	5 - 14	8 - 20	-58	249	189	218	0.641	2.35
QOMOS	3.9	2.98	4.3	5.6	196	2 - 9	2 - 3	Nan	Nan	Nan	115	0.797	4.11
Nyima	1.3	2.28	4.9	2.3	182	3 - 14	0 - 2	-13	56	36	194	0.631	2.02
Coqen	1.6	2.03	5.6	1.8	137	2 - 6	4 - 9	-15	146	260	155	0.821	3.94
MAWORS	0.8	2.23	4.3	1.0	107	1 - 9	1 - 29	-157	538	368	344	0.623	1.31
NADORS	2.4	1.88	3.5	3.0	64	12 - 48	20 - 50	-174	415	238	222	0.646	0.99
Burang	2.5	3.12	4.5	3.1	58	1 - 4	1 - 5	-65	100	33	121	0.659	4.10
Mangai	3.5	1.93	3.4	4.8	43	1 - 2	1 - 2	-3	69	20	76	0.747	8.32

Both air humidity (Q) and wind speed at a 20 m height (U_{20m}) at 15 stations show similar seasonal variations (Figures 2b and 2d). Generally, the seasonal patterns of Q and U_{20m} are influenced by the interaction of monsoon and westerly systems. Seasonally, the summer monsoon system lead to the lower values in U_{20m} and higher values in Q, while high values in U_{20m} and low values in Q during winter are coincident with the dominating westerly system. Spatially, Q decreases from southeast to northwest across the TP. Medog station, located in a subtropical forest climate, exhibits the highest annual average Q of 14.1 g m^{-3}. The higher group of annual average Q values are found at SETORS (5.61 g m^{-3}), Qamdo (4.28 g m^{-3}), and Mangkam (4.12 g m^{-3}), while the rest of the stations range from 1.74 to 3.67 g m^{-3}. Further, both the annual averages of Q and U_{20m} correlate with elevation, showing negative and positive correlations of -0.88 and 0.83, respectively (Figure S1). U_{20m} is the lowest in Medog, Qamdo, and SETORS, where wind speeds are generally under 2 m s^{-1}, primarily because of their locations in the southeast mountainous regions. Conversely, stations at higher elevations with more homogeneous landscapes, such as Nyima, Coqen, and Shuanghu, experience the highest wind speed.

3.2 The spatial-temporal variations of liquid precipitation and soil water content

The wet-dry condition at each station is mostly correlated with liquid precipitation and soil water content (Table 2). The highest annual precipitation occurs in the southeastern TP, at stations like Medog, SETORS, Mangkam, and Qamdo, where the monsoon system dominates. The monsoon system can bring moist air into the plateau, resulting in annual precipitation values of 2164 mm in Medog, 1053 mm in SETORS, 596 mm in Mangkam, and 456 mm in Qamdo. In contrast, stations with low annual precipitation, such as Mangai, Burang, NADORS, and MAWORS, are located in the western and northern parts of the TP, where mid-latitude westerlies prevail, with annual precipitation below 120 mm. The rest seven stations in the central and western TP, where both westerly and monsoon systems interact, experience annual precipitation ranging from 120 mm to 400 mm. Specifically, Baingoin, NAMORS, and Shuanghu, located in

https://doi.org/10.5194/essd-2025-195
Preprint. Discussion started: 12 June 2025
© Author(s) 2025. CC BY 4.0 License.

the central TP, receive annual precipitation of between 200 mm and 400 mm, while Nyima, Coqen, Gyirong, and QOMOS receive100 mm to 200 mm per year. This pattern of high in the southeast and low in the northwest aligns with the Global Precipitation Measurement (GPM) product [*G Li et al., 2021a*]. The spatial distribution of soil water content at depths of 10 cm and 160 cm generally mirrors the precipitation pattern, but they can be also influenced by soil properties and local conditions. For example, NADORS, situated near Bangong Co, exhibits the highest soil water content at 10 cm depth. At 160 cm depth, stations like Shuanghu, NADORS, MAWORS, and Gyirong show soil water content up to 0.20, indicating significant groundwater contribution. In contrast, Mangai, Burang, Coqen, and NAMORS have the lowest soil water contents. Thus, stations of Medog, SETORS, Mangkam, and Qamdo are classified as typical wet station and stations of QOMOS, Nyima, Coqen, Gyirong and MAWORS are considered as typical dry station.

Seasonally, liquid precipitation over the TP is primarily concentrated during the summer monsoon seasons, with peaks in July and August (Figure S3), consistent with findings from *Yang et al. [2023]* in central TP. *Chen et al. [2023]* observed that monthly precipitation in the Yarlung Tsangbo Grand Canyon exhibits two peaks, one in April and the other in August, which is also the case for SETORS and Medog. Diurnally, *P Li et al. [2021b]* noted that summer precipitation over the TP often occurs in the afternoon and evening. However, the diurnal patterns vary significantly across the 15 stations (Figure 3). Precipitation frequency and amounts followed similar diurnal variations, with notable exceptions at Baingoin and MAWORS, where precipitation frequency peaked between 6:00 and 11:00, but the highest rainfall amounts occurred at 14:00. At westerly-dominated stations in the northern TP like Mangai, NADORS, MAWORS, and Shuanghu, precipitation peaks during the day and is minimal at night, though the timing of these peaks varies. In contrast, stations in mountainous regions—Medog, Mangkam, Qamdo, Nyima, and Gyirong—experience peak precipitation mostly at night, similar to findings in *Chen et al. [2023]* for the Yarlung Zangbo Grand Canyon. SETORS, QOMOS, and Coqen exhibit bimodal precipitation patterns, with peaks at night and in the late afternoon. Burang and NAMORS show higher precipitation in the first half of the day, with lower amounts later, and such patterns are probably related with the lake breeze circulation. Generally, daytime rainfall is probably driven by up-slope flows due to surface heating, while the monsoon nocturnal low-level jet may contribute to nighttime rainfall. Further, the local circulations of lake-land breeze and mountain-valley breeze can also modulate the water circulations and impact on the diurnal variation of precipitation.

https://doi.org/10.5194/essd-2025-195
Preprint. Discussion started: 12 June 2025
© Author(s) 2025. CC BY 4.0 License.

Open Access Earth System Science Data Discussions

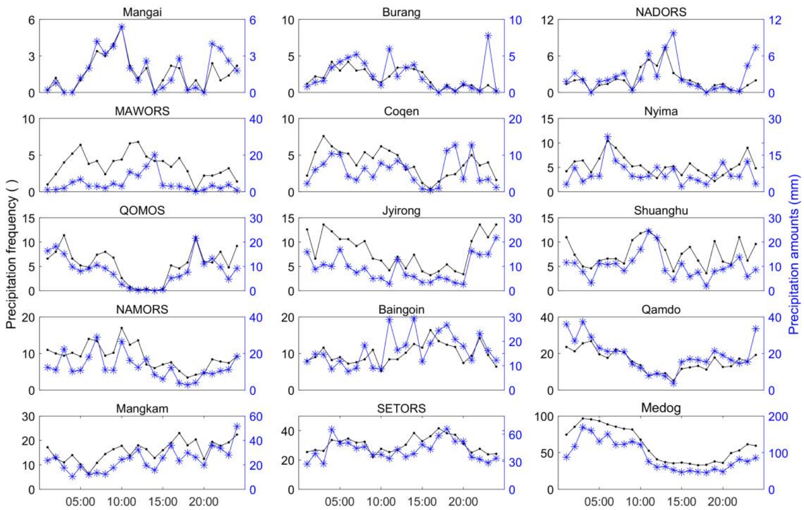

Figure 3. The diurnal variations of liquid precipitation amounts and frequency at 15 stations. Liquid precipitation frequency indicates the total times of liquid precipitation annually.

3.3 The spatial-temporal variations of energy budget flux

Net radiation (R_n) provides the energy source for LA energy and material exchange, and is mainly divided into three components: ground heat flux (G), *SH*, and *LE*. R_n generally shows positive values in its seasonal variations, indicating that the ground surface acts as a strong heat source relative to the overlying atmosphere. R_n peaks in June or July and reaches its lowest in December or January. SETORS and Gyirong have monthly R_n values of greater than 90 W m^2, while Baingoin and Mangai have values of below 70 W m^2. The other stations show values of between 70 and 90 W m^2, which are similar to those reported in previous studies, 4 stations over the TP and 4 stations in the lower reaches of the Yangtze River region [*Yao et al., 2024*]. Details for the seasonal variation of monthly net radiation and monthly ground heat flux and their annual means at the 15 stations can be found in Table S5-S6. Further, heat storage occurs mainly from March to August, peaking around June, while heat release is most significant from October to February, with the largest release in December. The annual average of monthly G ranges from -0.01 W m^2 at Qamdo to 2.39 W m^2 at NADORS. The close-to-zero G values suggest minimal impact of ground heat storage on the energy budget at an annual scale, while the dominating positive values suggest a warming trend in the ground, aligning with global warming and the rise in land surface temperature *[Duan and Xiao, 2015; Oku et al., 2006; C Zhang et al., 2023*].

https://doi.org/10.5194/essd-2025-195
Preprint. Discussion started: 12 June 2025
© Author(s) 2025. CC BY 4.0 License.

Earth System Science Data
Open Access Discussions

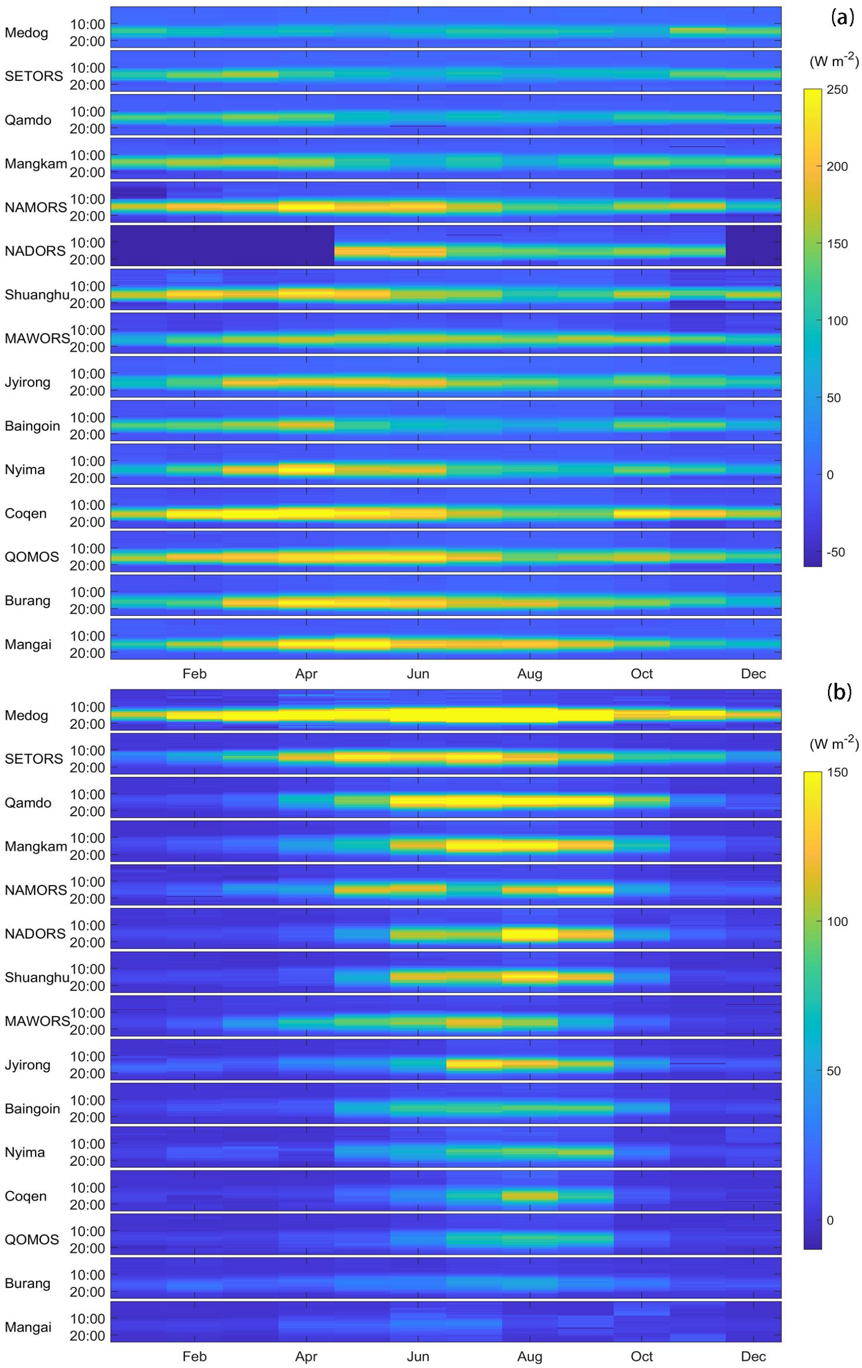

Figure 4. The heat maps for averaged diurnal and seasonal variations of sensible heat flux (a) and latent heat flux (b) at 15 stations.

© Author(s) 2025. CC BY 4.0 License.

Turbulent heat fluxes, including *SH* and *LE*, exhibit clear diurnal and seasonal variations (Figure 4), consistent with previous studies on the TP [*Y Ma et al.*, 2005; *Zhong et al.*, 2019a]. In addition, the seasonal evolution of monthly averaged diurnal *SH* and *LE* can be found in Figure S4-S5. *SH* peaks during the pre-monsoon months of April and May, and is lowest in the cold months of December and January. Stations with sufficient water availability, such as Medog, SETORS, Mangkam, Qamdo, Baingoin, MAWORS, and NADORS, have total annual *SH* values ranging from 269 to 356 W m^2. The first five stations receive high precipitation, while the latter two have substantial soil moisture supply. Other stations have total annual *SH* fluxes exceeding 400 W m^2, with QOMOS and Coqen reporting the highest annual values of 582 W m^2 and 626 W m^2, respectively. *LE* peaks during the monsoon seasons (July to August) and is not apparent throughout the cold months. Specifically, the total annual *LE* is only 61.3 W m^2 at the extremely dry Mangai station, while Medog records monthly *LE* values all exceeding 29 W m^2. Spatially, *LE* are showing decreasing pattern from the southeast wet regions to the northwest dry regions. As shown in Table 1, the *Bo* reflects the energy distribution between *SH* and *LE*. Medog, SETORS, and Qamdo in the southeast have *Bo* values of less than 1, indicating dominant heat consumption through the *LE*, while Mangai, Burang, and QOMOS in the northern and western regions have *Bo* ratios greater than 4, suggesting the dominant role of *SH*.

The energy budget closure ratio (*EBR*) is the ratio of turbulent energy fluxes (*SH* + *LE*) to available energy (R_n - *G*). The average *EBR* across the 15 stations is approximately 0.73, with values ranging from 0.62 to 1.04, where 11 stations have *EBR* values between 0.6 and 0.8, while Medog exceeds 1 (Table 1). These *EBR* values are consistent with the results from eddy flux stations globally [*Wilson et al.*, 2002]. The lack of perfect *EBR* can be attributed to several factors [*Foken, 2008; Mauder et al., 2020*], including (1) measurements footprint mismatch, (2) instrumental biases, (3) neglect of energy sinks like canopy heat storage, (4) loss of low- and high-frequency flux contributions, and (5) neglected scalar advection. Thus, as Medog station locates in the valley and has no ideal homogeneous flat environments, the EBR is inappropriately a little higher than 1.

Following the LA interaction theories, *SH* (*LE*) are primarily influenced by land-atmosphere temperature gradients or water vapor deficit ($\Delta T/\Delta E$), wind speed (*U*), soil moisture (SM) at 10 cm and 80 cm, land surface temperature (T_s) and net radiation (R_n), etc [*B Wang et al., 2017*]. The correlation coefficients between *SH* (*LE*) and the related variables can be found in Table S7, and the dominating factors for LA turbulent flux are significantly different under dry and wet stations, where energy-related variables are most important in water-sufficient conditions, while water-related variables show dominant role in water-shortage conditions. For example, stations like Medog, SETORS, Mangkam, and Qamdo, which are located in the southeast TP and receive substantial precipitation, show higher correlations of *LE* with R_n and T_s than with soil moisture. On the contrary, dry stations like QOMOS, Nyima, Coqen, MAWORS have higher correlation coefficients of *LE* with soil moisture at 10 cm than others. Mangai, an extremely dry station with annual precipitation value of only 43.2 mm and very low soil moisture conditions (0.01-0.02), has the smallest annual *ET* value and no significant correlations with all the variables. In NADORS, the annual ET has a value of 222.4 mm, significantly higher than the annual precipitation amount of 64 mm, and the volumetric water content at 80 cm (*SM* 80cm) can reach up to 0.3, suggesting a

https://doi.org/10.5194/essd-2025-195
Preprint. Discussion started: 12 June 2025
© Author(s) 2025. CC BY 4.0 License.

substantial impact of groundwater supply. Thus, soil moisture and R_n have comparable high correlation coefficients in NADORS.

The correlation coefficients between *SH* (*LE*) and related environment variables under conditions of all stations, wet stations (Medog, SETORS, Mangkam, and Qamdo) and dry stations (QOMOS, Nyima, Coqen, Gyirong) are grouped in Figure 5. For all stations included, *SH* variations are primarily driven by ΔT, followed by R_n and T_s, with correlation coefficients of 0.57, 0.55 and 0.34, respectively (Figure 5a). Further, *SH* has a positive correlation with wind speed and a negative correlation with soil moisture. The correlation coefficients show large diversity under dry and wet conditions, with generally lower values in wet stations than those in dry stations. For example, the averaged correlation coefficients between *SH* and $\Delta T/R_n/T_s$ under dry stations are 0.63/0.65/0.44 while those values (0.32/0.40/0.13) are much smaller under wet conditions. Wind speed has weaker correlation with *SH.* but in MAWORS and Medog, the correlation coefficients could approach to 0.5. In NAMORS, there is a negative correlation between wind speed and *SH.* These phenomenons may be related with the local circulations of mountain-valley breeze and lake-land breeze, which may lead to synchronized and opposite variations in such conditions.

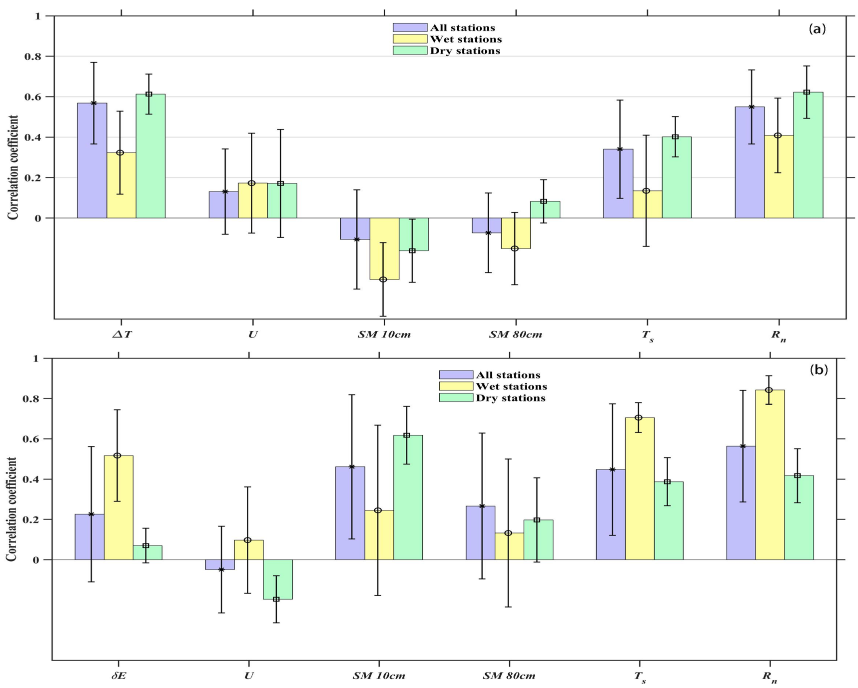

Figure 5. The correlation coefficients between sensible heat flux (a), latent heat flux (b) and related environmental variables at a temporal resolution of hourly under conditions of all stations, wet stations and dry stations, respectively.

https://doi.org/10.5194/essd-2025-195
Preprint. Discussion started: 12 June 2025
© Author(s) 2025. CC BY 4.0 License.

The correlations between LE and environmental variables are more complex (Table S7 and Figure 5b). The three paramount factors are R_n, T_s and soil moisture at 10 cm, with correlation coefficients of 0.56, 0.46, 0.45, respectively. For wet stations, the most important variables are energy related variables (R_n and T_s). Stations such as Medog, Mangkam, SETORS, Qamdo, Gyirong, and NADORS follow this pattern, with the first four stations influenced by high precipitation and the latter two by soil water content. ΔE represents the difference between the actual moisture content of air and the moisture it could hold at saturation. At higher temperatures, the amount of moisture required for saturation is double that at lower temperatures. Thus, ΔE shows significant high correlations at Medog and SETORS. At dry stations like Burang, Nyima, MAWORS, and Coqen, the most influential variable is soil moisture, followed by R_n and T_s. Thus, both energy and water availability play dominant roles. At extremely dry station of Mangai, most of the monthly LE values are close to zero, and none of the variations show significant correlations with LE. For QOMOS, the largest correlation with LE is seen with soil moisture at 10 cm, suggesting that water availability plays a more critical role in ET than energy availability in this region.

In a brief summary, R_n and T_s are continuously important factors for land-atmosphere turbulent heat flux exchange over TP; for *SH*, ΔT plays a dominant role and soil moisture may show negative correlations under wet conditions; for *LE*, water vapor deficit show important influences under wet conditions while soil moisture show significance under dry conditions.

3.4 The seasonal variations of *NEE*, *GPP* and *Re*

The seasonal variations of daily *NEE*, *GPP*, and *Res* averaged over the observational period show significant differences across sites, and the sites with relatively good vegetation coverage follow a single-peak distribution pattern, i.e. SETORS, Qamdo, Mangkam, etc., but the other sites, including Burang, Nyima, Coqen, Mangai, show weak or nearly non seasonal variations (Figure 6 and Table 2). The carbon absorption and release are determined by vegetation photosynthesis process and ecosystem respiration. The seasonal variation of carbon fluxes follow the vegetation growth, with highest values during the summer peak growing seasons. For example, stations with substantial vegetation growth, such as SETORS, Qamdo, Mangkam, NADORS, and MAWORS, exhibit higher peaks and fluctuations in *NEE*, *GPP*, and *Re*. The first three stations benefit from high precipitation, while the latter two stations receive significant shallow soil water supply from surrounding lakes or glaciers. These five stations exhibit strong carbon sink capacities, with *NEE* values all smaller than -120 g C m^{-2} during the growing season. Specifically, NADORS shows the largest *NEE* value of -174 g C m^{-2} from May to October, while SETORS has the highest daily *NEE* values, exceeding 6 g C m^{-2} d^{-1}. Similarly, *GPP* and *Re* values at the 5 stations all exceed 400 g C m^{-2} and 190 g C m^{-2}, with SETORS having the highest *GPP* and *Re* values of 754 g C m^{-2} and 633 g C m^{-2}, respectively, due to its favorable temperature and water conditions for vegetation growth. In water-limited regions like Mangai and Nyima, carbon fluxes fluctuations are minimal. Daily *NEE* values remain below 0.5 g C m^{-2} d^{-1}, even during the growing season. The total annual *NEE* values are -3.2 g C m^{-2} and -12.8 g C m^{-2} in Mangai and Nyima, respectively. *GPP* and *Re* values are also low, with annual totals below 70 g C m^{-2} for *GPP* and 40 g C m^{-2} for *Re*. The smallest annual *GPP* value is 56 g C m^{-2} at Nyima, and the smallest annual *Re* value is 20 g C m^{-2} at Mangai. Although annual *NEE* values at SETORS and MAWORS are relatively similar,

https://doi.org/10.5194/essd-2025-195
Preprint. Discussion started: 12 June 2025
© Author(s) 2025. CC BY 4.0 License.

SETORS has much larger *GPP* and *Re* values because of the efficient water supply and warm climate. In contrast, *[Y Wang et al., 2021]* reported NADORS with average *GPP* value of 1.60 g C m^{-2} d^{-1} and average *Re* value of 0.71 g C m^{-2} d^{-1} during growing season of 2014-2015, while these values (2.93 g C m^{-2} d^{-1} for *GPP* and 1.35 g C m^{-2} d^{-1} for *Re*) are much larger during growing season of 2021-2022 in our estimation. In addition, the maximum net carbon uptake has a value of -2.1 g C m^{-2} d^{-1} in MAWORS during 2015-2016 *[Y Wang et al., 2021],* however, the largest *NEE* exchange value is -2.6 g C m^{-2} d^{-1} in our measurements. Thus, it may indicate the improvement of vegetation status in the two western stations during the past 10 years *[Zhong et al., 2019b]*.

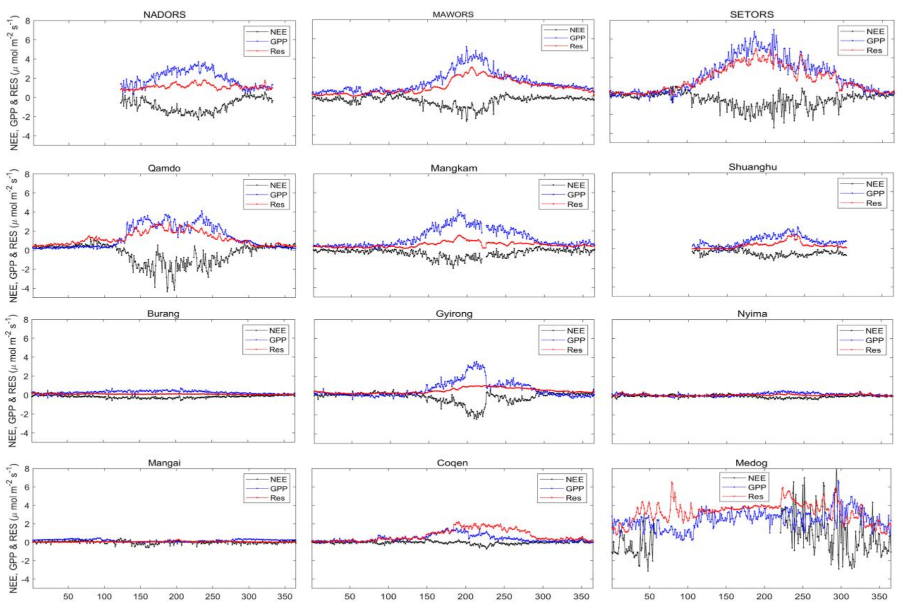

Figure 6. The seasonal variations in *GPP*, *Re*, *NEE* across different sites. The negative *NEE* values indicated a net uptake of CO_2. (The black, blue and red line stand for daily *NEE*, *GPP* and *Re*, respectively).

The annual *NEE* values are negative at 11 out of 12 stations, with exceptions at Medog (Table 1). The annual *NEE* values at the stations of Qamdo, SETORS, Mangkam, MAWORS and NADORS all smaller than -120 g C, coincident with stations with higher *ET* annual values, suggesting the significance of water-carbon coupling in land-atmosphere interaction process. At stations of Shuanghu, Burang, Jyirong, the annual *NEE* values are between -50 g C and -100 g C and the rest stations of Nyima and Mangai have annual *NEE* values of close to carbon neutral. At Medog, despite substantial carbon absorption during the daytime, significant carbon release at night caused by soil respiration leads to large carbon release. Mangai, with sparse vegetation, functions nearly as carbon neutral. An obvious drastic variation of *NEE* values during August at Gyirong station can be found and it corresponds to a soil drought event caused by water deficit. The water deficit event results in decrease in *NEE* and *LE* and obvious increase in T_s and *SH*. Notably, carbon absorption primarily occur during summer growing seasons of May to September and function as carbon neutral during winter seasons. The spatial distribution of annual NEE values generally follow the distribution of water conditions, where sufficient water can promote

https://doi.org/10.5194/essd-2025-195
Preprint. Discussion started: 12 June 2025
© Author(s) 2025. CC BY 4.0 License.

vegetation growth, allowing photosynthesis to absorb more CO_2 than respiration releases [*Wang et al., 2021; Wang et al., 2023*].

Global forests have been widely recognized as carbon sinks [*Hubau et al.*, 2020; *Pan et al., 2024*]. Medog station, located in the Yarlung Zangbo River valley, is surrounded by subtropical vegetation and forests and has an annual *NEE* value of 365 g C, indicating that the land cover acts as an obvious carbon source. Studies have indicated that tropical forests can become carbon sources due to factors such as deforestation, soil respiration exceeding photosynthesis, lingering droughts, and extreme warming [*Gatti et al., 2021; Mills et al., 2023; Xie et al., 2016*]. During a severe drought in the summer of 2013 in a subtropical forest in China, the ecosystem switched to a net carbon source by late August [*Xie et al., 2016*]. Similarly, *Mills et al. [2023]* found that tropical forests, after deforestation and degradation, can act as net carbon sources. The Medog station, characterized by a hot climate and complex terrain, is under construction at the southern flat areas, resulting in vegetation destruction. The hot environment, coupled with limited solar radiation exposure due to the surrounding steep terrain, may reduce photosynthesis and promote carbon loss from soil and microorganism respiration [*Wang et al., 2021; Wang et al., 2023*]. Although *NEE* values can be significantly negative during the daytime due to photosynthesis, obvious and long-lasting ecosystem respiration at night leads to a net carbon release (Figure S6).

4 Summary

The establishment of a comprehensive observation and research platform marks a significant advancement in understanding land-atmosphere water, heat and CO_2 flux across diverse stations. The platform features standardized configurations at each station, including an EC system, a 20 m PBL tower measuring wind, temperature, and humidity across five layers, soil moisture and temperature probes at five depths, energy budget probes for radiation components and soil heat flux, a thermal infrared temperature probe, a barometer, and a rain gauge. It covers a range of landscapes such as alpine steppe, alpine meadow, grassland, bare ground, forest, and desert. The observation platform aims to provide long-term, standardized, high-quality data on land-atmosphere interaction processes over the TP, with a particular focus on the data-scarce regions of the western TP. The extensive hydrometeorological dataset offers initial insights into the spatial and temporal variations of meteorological conditions, liquid precipitation, and turbulent fluxes. Diurnal precipitation patterns reveal three types: peak at night, peak during the day, and bimodal peaks. While liquid precipitation can distinguish between water-limited and energy-limited regions, soil moisture—both from surface and deeper layers—also plays a key role in ET, as seen in stations like NADORS and Shuanghu. NEE fluxes are near zero at bare ground stations, show significant carbon release in forested areas under construction, and function as carbon sinks in most alpine meadows and alpine steppe sites. This platform is critical for supporting scientific research and sustainable development. However, challenges remain in capturing data from remote and heterogeneous regions, as well as limitations in current technologies. Scaling flux towers for global models remains difficult, highlighting the need for robust interpolation and validation techniques. Additionally, further investigation is required to understand the impacts of land-use changes, such as deforestation and reforestation, on turbulent heat fluxes and their feedback to the climate system.

© Author(s) 2025. CC BY 4.0 License.

Competing interests

The authors declare that they have no conflict of interests.

Author contribution

BBW and YMM jointly led the writing of this article and were responsible for the establishment and maintenance of the experimental sites and instrumentation. BBW took the lead in dataset consolidation, processed the data into the standardized format described in this study, and drafted the manuscript in collaboration with all co-authors. ZYH, WQM, XLC, CBH, ZPX, YYW, MSL, BM, XDS, WML, and ZLC contributed to the maintenance of the observation systems, data analysis, and provided critical feedback and revisions to the manuscript.

Data availability statement

The hourly dataset including air temperature, air humidity, wind speed, land surface temperature, soil moisture, downward shortwave radiation, downward longwave radiation, upward shortwave radiation, upward longwave radiation, sensible heat flux, latent heat flux, Net ecosystem change can be downloaded freely in the Tibetan Plateau Data Center. The DOI of the dataset is https://doi.org/10.11888/Atmos.tpdc.302428. The data can be referenced by Wang and Ma (2025). The web link is https://data.tpdc.ac.cn/en/disallow/e8032ff8-2437-4363-876f-2af4e4558a4d.

Acknowledgement

This research was jointly funded by the National Key Research and Development Program of China (2023YFF0805300), the National Natural Science Foundation of China (Grant Nos. U2442213 and 42230610), the Youth Innovation Promotion Association of the Chinese Academy of Sciences (Grant No. 2022069), the Second Tibetan Plateau Scientific Expedition and Research Program (Grant No. 2019QZKK0103).

References

André, J.-C., J.-P. Goutorbe, and A. Perrier (1986), HAPEX—MOBILHY: A Hydrologic Atmospheric Experiment the Study of Water Budget and Evaporation Flux at the Climatic Scale, *Bulletin of the American Meteorological Society*, *67*(2), 138-144, doi:https://doi.org/10.1175/1520-0477-67.2.138.

Baldocchi, D. (2014), Measuring fluxes of trace gases and energy between ecosystems and the atmosphere – the state and future of the eddy covariance method, *Global Change Biology*, *20*(12), 3600-3609, doi:https://doi.org/10.1111/gcb.12649.

Bei, N., L. Zhao, J. Wu, X. Li, T. Feng, and G. Li (2018), Impacts of sea-land and mountain-valley circulations on the air pollution in Beijing-Tianjin-Hebei (BTH): A case study, *Environmental Pollution*, *234*, 429-438, doi:https://doi.org/10.1016/j.envpol.2017.11.066.

Chen, X., D. Cao, Y. Liu, X. Xu, and Y. Ma (2023), An observational view of rainfall characteristics and evaluation of ERA5 diurnal cycle in the Yarlung Tsangbo Grand Canyon, China, *Quarterly Journal of the Royal Meteorological Society*, *149*(753), 1459-1472, doi:https://doi.org/10.1002/qj.4468.

Duan, A., and Z. Xiao (2015), Does the climate warming hiatus exist over the Tibetan Plateau?, *Scientific Reports*, *5*(1), 13711, doi:10.1038/srep13711.

Foken, T. (2008), THE ENERGY BALANCE CLOSURE PROBLEM: AN OVERVIEW, *Ecological Applications*, *18*(6), 1351-1367, doi:https://doi.org/10.1890/06-0922.1.

Friedlingstein, P., et al. (2022), Global Carbon Budget 2022, *Earth Syst. Sci. Data*, *14*(11), 4811-4900, doi:10.5194/essd-14-4811-2022.

Gatti, L. V., et al. (2021), Amazonia as a carbon source linked to deforestation and climate change, *Nature*, *595*(7867), 388-393, doi:10.1038/s41586-021-03629-6.

Gentine, P., A. Massmann, B. R. Lintner, S. Hamed Alemohammad, R. Fu, J. K. Green, D. Kennedy, and J. Vilà-Guerau de Arellano (2019), Land–atmosphere interactions in the tropics – a review, *Hydrol. Earth Syst. Sci.*, *23*(10), 4171-4197, doi:10.5194/hess-23-4171-2019.

Gerken, T., T. Biermann, W. Babel, M. Herzog, Y. Ma, T. Foken, and H.-F. Graf (2014), A modelling investigation into lake-breeze development and convection triggering in the Nam Co Lake basin, Tibetan Plateau, *Theoretical and Applied Climatology*, *117*(1), 149-167, doi:10.1007/s00704-013-0987-9.

Goutorbe, J. P., et al. (1997), An overview of HAPEX-Sahel: a study in climate and desertification, *Journal of Hydrology*, *188-189*, 4-17, doi:https://doi.org/10.1016/S0022-1694(96)03308-2.

Halldin, S., S. E. Gryning, L. Gottschalk, A. Jochum, L. C. Lundin, and A. A. Van de Griend (1999), Energy, water and carbon exchange in a boreal forest landscape — NOPEX experiences, *Agricultural and Forest Meteorology*, *98-99*, 5-29, doi:https://doi.org/10.1016/S0168-1923(99)00148-3.

Huang, J., et al. (2023), Global Climate Impacts of Land-Surface and Atmospheric Processes Over the Tibetan Plateau, *Reviews of Geophysics*, *61*(3), e2022RG000771, doi:https://doi.org/10.1029/2022RG000771.

Hubau, W., et al. (2020), Asynchronous carbon sink saturation in African and Amazonian tropical forests, *Nature*, *579*(7797), 80-87, doi:10.1038/s41586-020-2035-0.

Li, G., Z. Yu, W. Wang, Q. Ju, and X. Chen (2021a), Analysis of the spatial Distribution of precipitation and topography with GPM data in the Tibetan Plateau, *Atmospheric Research*, *247*, 105259, doi:https://doi.org/10.1016/j.atmosres.2020.105259.

Li, L., R. Zhang, P. Wu, M. Wen, and J. Duan (2020), Roles of Tibetan Plateau vortices in the heavy rainfall over southwestern China in early July 2018, *Atmospheric Research*, *245*, 105059, doi:https://doi.org/10.1016/j.atmosres.2020.105059.

Li, P., K. Furtado, T. Zhou, H. Chen, and J. Li (2021b), Convection-permitting modelling improves simulated precipitation over the central and eastern Tibetan Plateau, *Quarterly Journal of the Royal Meteorological Society*, *147*(734), 341-362, doi:https://doi.org/10.1002/qj.3921.

Liu, S., et al. (2018), The Heihe Integrated Observatory Network: A Basin-Scale Land Surface Processes Observatory in China, *Vadose Zone Journal*, *17*(1), 180072, doi:https://doi.org/10.2136/vzj2018.04.0072.

Lü, D., Z. Chen, G. Wang, J. Chen, J. Ji, Y. Li, and H. Chen (1997), Inner Mongolia Semi-Arid Grassland Soil-Vegetation-Atmosphere Interaction, *Climatic and Environmental Research*, *2*(3), 199-209, doi:10.3878/j.issn.1006-9585.1997.03.01.

Ma, N., and Y. Zhang (2022), Increasing Tibetan Plateau terrestrial evapotranspiration primarily driven by precipitation, *Agricultural and Forest Meteorology*, *317*, 108887, doi:https://doi.org/10.1016/j.agrformet.2022.108887.

Ma, Y., S. Fan, H. Ishikawa, O. Tsukamoto, T. Yao, T. Koike, H. Zuo, Z. Hu, and Z. Su (2005), Diurnal and inter-monthly variation of land surface heat fluxes over the central Tibetan Plateau area, *Theoretical and Applied Climatology*, *80*(2), 259-273, doi:10.1007/s00704-004-0104-1.

https://doi.org/10.5194/essd-2025-195
Preprint. Discussion started: 12 June 2025
© Author(s) 2025. CC BY 4.0 License.

Ma, Y., et al. (2020), A long-term (2005–2016) dataset of hourly integrated land–atmosphere interaction observations on the Tibetan Plateau, *Earth Syst. Sci. Data*, *12*(4), 2937-2957, doi:10.5194/essd-12-2937-2020.

Ma, Y., Y. Wang, and C. Han (2018), Regionalization of land surface heat fluxes over the heterogeneous landscape: from the Tibetan Plateau to the Third Pole region, *International Journal of Remote Sensing*, *39*(18), 5872-5890, doi:10.1080/01431161.2018.1508923.

Ma, Y., et al. (2024), Dataset of spatially extensive long-term quality-assured land–atmosphere interactions over the Tibetan Plateau, *Earth Syst. Sci. Data*, *16*(6), 3017-3043, doi:10.5194/essd-16-3017-2024.

Ma, Y., et al. (2023), Comprehensive study of energy and water exchange over the Tibetan Plateau: A review and perspective: From GAME/Tibet and CAMP/Tibet to TORP, TPEORP, and TPEITORP, *Earth-Science Reviews*, *237*, 104312, doi:https://doi.org/10.1016/j.earscirev.2023.104312.

Ma, Y. M., S. C. Kang, L. P. Zhu, B. Q. Xu, L. D. Tian, and T. D. Yao (2008), TIBETAN OBSERVATION AND RESEARCH PLATFORM Atmosphere-Land Interaction over a Heterogeneous Landscape, *Bull.amer.meteor.soc*, *89*(10), 1487-1492.

Massman, W. J., and X. Lee (2002), Eddy covariance flux corrections and uncertainties in long-term studies of carbon and energy exchanges, *Agricultural and Forest Meteorology*, *113*(1), 121-144, doi:https://doi.org/10.1016/S0168-1923(02)00105-3.

Mauder, M., M. Cuntz, C. Drüe, A. Graf, C. Rebmann, H. P. Schmid, M. Schmidt, and R. Steinbrecher (2013), A strategy for quality and uncertainty assessment of long-term eddy-covariance measurements, *Agricultural and Forest Meteorology*, *169*, 122-135, doi:https://doi.org/10.1016/j.agrformet.2012.09.006.

Mauder, M., and T. Foken (2006), Impact of post-field data processing on eddy covariance flux estimates and energy balance closure, *Meteorologische Zeitschrift*, *15*(6), 597-609.

Mauder, M., T. Foken, and J. Cuxart (2020), Surface-Energy-Balance Closure over Land: A Review, *Boundary-Layer Meteorology*, *177*(2), 395-426, doi:10.1007/s10546-020-00529-6.

Mills, M. B., et al. (2023), Tropical forests post-logging are a persistent net carbon source to the atmosphere, *Proceedings of the National Academy of Sciences*, *120*(3), e2214462120, doi:doi:10.1073/pnas.2214462120.

Oku, Y., H. Ishikawa, S. Haginoya, and Y. Ma (2006), Recent Trends in Land Surface Temperature on the Tibetan Plateau, *Journal of Climate*, *19*(12), 2995-3003, doi:https://doi.org/10.1175/JCLI3811.1.

Pan, Y., Birdsey, R.A., Phillips, O.L. et al. The enduring world forest carbon sink. Nature 631, 563–569 (2024)

Qi, Y., D. Wei, H. Zhao, and X. Wang (2021), Carbon Sink of a Very High Marshland on the Tibetan Plateau, *Journal of Geophysical Research: Biogeosciences*, *126*(4), e2020JG006235, doi:https://doi.org/10.1029/2020JG006235.

Santanello, J. A., et al. (2018), Land–Atmosphere Interactions: The LoCo Perspective, *Bulletin of the American Meteorological Society*, *99*(6), 1253-1272, doi:https://doi.org/10.1175/BAMS-D-17-0001.1.

Sellers, P., et al. (1995), The Boreal Ecosystem–Atmosphere Study (BOREAS): An Overview and Early Results from the 1994 Field Year, *Bulletin of the American Meteorological Society*, *76*(9), 1549-1577, doi:https://doi.org/10.1175/1520-0477(1995)076<1549:TBESAO>2.0.CO;2.

Sellers, P. J., F. G. Hall, G. Asrar, D. E. Strebel, and R. E. Murphy (1992), An overview of the First International Satellite Land Surface Climatology Project (ISLSCP) Field Experiment (FIFE), *Journal of Geophysical Research: Atmospheres*, *97*(D17), 18345-18371, doi:https://doi.org/10.1029/92JD02111.

https://doi.org/10.5194/essd-2025-195
Preprint. Discussion started: 12 June 2025
© Author(s) 2025. CC BY 4.0 License.

Seo, Y.-W., and K.-J. Ha (2022), Changes in land-atmosphere coupling increase compound drought and heatwaves over northern East Asia, *npj Climate and Atmospheric Science*, *5*(1), 100, doi:10.1038/s41612-022-00325-8.

Suni, T., et al. (2015), The significance of land-atmosphere interactions in the Earth system—iLEAPS achievements and perspectives, *Anthropocene*, *12*, 69-84, doi:https://doi.org/10.1016/j.ancene.2015.12.001.

Turetsky, M. R., et al. (2020), Carbon release through abrupt permafrost thaw, *Nature Geoscience*, *13*(2), 138-143, doi:10.1038/s41561-019-0526-0.

Twine, T. E., W. P. Kustas, J. M. Norman, D. R. Cook, P. R. Houser, T. P. Meyers, J. H. Prueger, P. J. Starks, and M. L. Wesely (2000), Correcting eddy-covariance flux underestimates over a grassland, *Agricultural and Forest Meteorology*, *103*(3), 279-300, doi:https://doi.org/10.1016/S0168-1923(00)00123-4.

Wang, Shuzhou, and Yaoming (2011), Characteristics of Land-Atmosphere Interaction Parameters over the Tibetan Plateau, *Journal of Hydrometeorology*.

Wang, B., Y. Ma, W. Ma, and Z. Su (2017), Physical controls on half-hourly, daily, and monthly turbulent flux and energy budget over a high-altitude small lake on the Tibetan Plateau, *Journal of Geophysical Research: Atmospheres*, *122*(4), 2289-2303, doi:https://doi.org/10.1002/2016JD026109.

Wang, B., Ma, Y. (2025). Meteorological variables and eddy fluxes at 15 land-atmosphere interaction stations over the Tibetan Plateau (May-2021 to July 2023). National Tibetan Plateau / Third Pole Environment Data Center. https://doi.org/10.11888/Atmos.tpdc.302428.

Wang, Y., J. Xiao, Y. Ma, J. Ding, X. Chen, Z. Ding, and Y. Luo (2023a), Persistent and enhanced carbon sequestration capacity of alpine grasslands on Earth's Third Pole, *Science Advances*, *9*.

Wang, Y., J. Xiao, Y. Ma, J. Ding, X. Chen, Z. Ding, and Y. Luo (2023b), Persistent and enhanced carbon sequestration capacity of alpine grasslands on Earth's Third Pole, *Science Advances*, *9*(20), eade6875, doi:doi:10.1126/sciadv.ade6875.

Wang, Y., J. Xiao, Y. Ma, Y. Luo, Z. Hu, F. Li, Y. Li, L. Gu, Z. Li, and L. Yuan (2021), Carbon fluxes and environmental controls across different alpine grassland types on the Tibetan Plateau, *Agricultural and Forest Meteorology*, *311*, 108694, doi:https://doi.org/10.1016/j.agrformet.2021.108694.

Wei, D., Y. Qi, Y. Ma, X. Wang, W. Ma, T. Gao, L. Huang, H. Zhao, J. Zhang, and X. Wang (2021), Plant uptake of CO₂ outpaces losses from permafrost and plant respiration on the Tibetan Plateau, *Proceedings of the National Academy of Sciences*, *118*(33), e2015283118, doi:doi:10.1073/pnas.2015283118.

Wilson, K., et al. (2002), Energy balance closure at FLUXNET sites, *Agricultural and Forest Meteorology*, *113*(1), 223-243, doi:https://doi.org/10.1016/S0168-1923(02)00109-0.

Wu, G., and Y. Zhang (1998), Tibetan Plateau Forcing and the Timing of the Monsoon Onset over South Asia and the South China Sea, *Monthly Weather Review*, *126*(4), 913-927.

Wu, G., et al. (2023), An Integrated Research Plan for the Tibetan Plateau Land–Air Coupled System and Its Impacts on the Global Climate, *Bulletin of the American Meteorological Society*, *104*(1), E158-E177, doi:https://doi.org/10.1175/BAMS-D-21-0293.1.

Wutzler, T., A. Lucas-Moffat, M. Migliavacca, J. Knauer, K. Sickel, L. Šigut, O. Menzer, and M. Reichstein (2018), Basic and extensible post-processing of eddy covariance flux data with REddyProc, *Biogeosciences*, *15*(16), 5015-5030, doi:10.5194/bg-15-5015-2018.

https://doi.org/10.5194/essd-2025-195
Preprint. Discussion started: 12 June 2025
© Author(s) 2025. CC BY 4.0 License.

Xie, Z., L. Wang, B. Jia, and X. Yuan (2016), Measuring and modeling the impact of a severe drought on terrestrial ecosystem CO_2 and water fluxes in a subtropical forest, *Journal of Geophysical Research: Biogeosciences*, *121*(10), 2576-2587, doi:https://doi.org/10.1002/2016JG003437.

Xu, X., and L. Chen (2006), Advances of the Study on Tibetan Plateau Experiment of Atmospheric Sciences, *Journal of Applied Meteorological Science*, *17*(6), 756-772.

Yang, K., et al. (2023), Cross-sectional rainfall observation on the central-western Tibetan Plateau in the warm season: System design and preliminary results, *Science China Earth Sciences*, *66*(5), 1015-1030, doi:10.1007/s11430-022-1081-4.

Yang, K., T. Koike, H. Ishikawa, O. Kim, X. Li, H. Liu, S. Liu, M. A. Yaoming, and J. Wang (2008), Turbulent Flux Transfer over Bare-Soil Surfaces; Characteristics and Parameterization, *Journal of Applied Meteorology and Climatology*(1), 47.

Yao, N., Y. Ma, B. Wang, J. Zou, J. Sun, and Z. Xie (2024), A comparative study of the land–atmosphere energy and water exchanges over the Tibetan Plateau and the Yangtze River Region, *Atmospheric and Oceanic Science Letters*, *17*(2), 100447, doi:https://doi.org/10.1016/j.aosl.2023.100447.

Ye, D.-Z., and G.-X. Wu (1998), The role of the heat source of the Tibetan Plateau in the general circulation, *Meteorology and Atmospheric Physics*, *67*(1), 181-198, doi:10.1007/BF01277509.

Yu, G.-R., Z. Chen, and Y.-P. Wang (2024), Carbon, water and energy fluxes of terrestrial ecosystems in China, *Agricultural and Forest Meteorology*, *346*, 109890, doi:https://doi.org/10.1016/j.agrformet.2024.109890.

Yuan, L., X. Chen, Y. Ma, C. Han, B. Wang, and W. Ma (2024), Long-term monthly 0.05° terrestrial evapotranspiration dataset (1982–2018) for the Tibetan Plateau, *Earth Syst. Sci. Data*, *16*(2), 775-801, doi:10.5194/essd-16-775-2024.

Yuan, L., Y. Ma, X. Chen, Y. Wang, and Z. li (2021), An Enhanced MOD16 Evapotranspiration Model for the Tibetan Plateau During the Unfrozen Season, *Journal of Geophysical Research: Atmospheres*, *126*, doi:10.1029/2020JD032787.

Zhang, C., D.-H. Qin, and P.-M. Zhai (2023), Amplification of warming on the Tibetan Plateau, *Advances in Climate Change Research*, *14*(4), 493-501, doi:https://doi.org/10.1016/j.accre.2023.07.004.

Zhang, Y., N. Wagner, K. Goergen, and S. Kollet (2024), Summer evapotranspiration-cloud feedbacks in land-atmosphere interactions over Europe, *Climate Dynamics*, doi:10.1007/s00382-024-07475-w.

Zhao, L., Y. Li, X. Zhao, S. Xu, Y. Tang, G. Yu, S. Gu, M. Du, and Q. Wang (2005), Comparative study of the net exchange of CO_2 in 3 types of vegetation ecosystems on the Qinghai-Tibetan Plateau, *Chinese Science Bulletin*, *50*(16), 1767-1774, doi:10.1360/04wd0316.

Zhong, L., Y. Ma, Z. Hu, Y. Fu, Y. Hu, X. Wang, M. Cheng, and N. Ge (2019), Estimation of hourly land surface heat fluxes over the Tibetan Plateau by the combined use of geostationary and polar-orbiting satellites, *Atmos. Chem. Phys.*, *19*(8), 5529-5541, doi:10.5194/acp-19-5529-2019.

Zhu, L., Z. Meng, F. Zhang, and P. M. Markowski (2017), The influence of sea- and land-breeze circulations on the diurnal variability in precipitation over a tropical island, *Atmos. Chem. Phys.*, *17*(21), 13213-13232, doi:10.5194/acp-17-13213-2017.